ACS OMEGA

http://pubs.acs.org/journal/acsodf

Article

A New Systematic Construction of Novel Three-Dimensional Spin Crossover Coordination Polymers Based on the $[Ag^{I}_{2}(CN)_{3}]$ Building Unit

Takashi Kosone,* Syogo Okuda, Masaya Kawata, Shunsuke Arai, Ryota Kosuge, and Takeshi Kawasaki

Cite This: *ACS Omega* 2021, 6, 12187−12193

Read Online

ACCESS | Metrics & More | Article Recommendations | Supporting Information

ABSTRACT: New three-dimensional spin crossover (SCO) coordination polymers systematically constructed by the novel building unit $[Ag^{I}_{2}(CN)_{3}]$, Fe^{II}(3-Br-5-CH_3pyridine)$_2[Ag^{I}_{2}(CN)_{3}][Ag^{I}(CN)_{2}]$ (**1**), Fe^{II}(3-Br-5-Clpyridine)$_2[Ag^{I}_{2}(CN)_{3}][Ag^{I}(CN)_{2}]$ (**2**), and Fe^{II}(3,5-Brpyridine)$_2[Ag^{I}_{2}(CN)_{3}][Ag^{I}(CN)_{2}]$ (**3**), have been synthesized and characterized. The bismonodentate binuclear $[Ag_2(CN)_3]^-$ and mononuclear $[Ag^{I}(CN)_2]^-$ units and Fe^{II} atoms assemble to form a 3D network structure. The structures of **1**−**3** are crystallographically identical, which made up the triply interpenetration combined with complicated intermolecular interactions including Ag···Ag, Ag···X (pyridine substituents) and π-stacking interactions. Magnetic and differential scanning calorimetry studies were performed for **1**−**3**. These compounds display a similar SCO behavior, while the critical temperatures (T_c) are shifted by the substituent effect. Due to the identical structures of **1**−**3**, the order of T_c clearly corresponds with the Hammett constant.

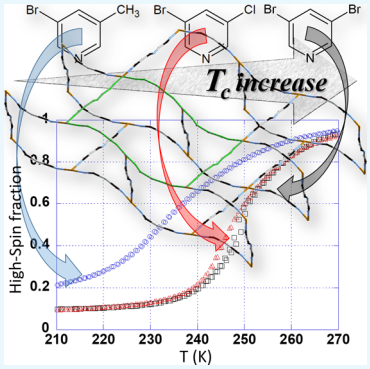

1. INTRODUCTION

Coordination chemistry associated with d- and f-block complexes attracts much attention from various forms of chemistry such as photochemistry, electrochemistry, catalyst chemistry, radiochemistry, and magnetochemistry.[1] In particular, the Fe(II) spin crossover (SCO) phenomenon for developing practical molecular magnetic devices is one of the most attractive research areas. It is necessary to construct a strong cooperative interaction between Fe centers and optimize the ligand field strength of the FeN_6 coordination environment.[2] Particularly, the strong cooperativity creates a hysteresis loop between the high-spin (HS) state and low-spin (LS) state, which is the most important part of the memory effect. Therefore, the design and synthesis of new SCO coordination polymers (CPs) are fundamental steps to develop the practical SCO materials. Up to now, a huge number of two-dimensional (2D) and three-dimensional (3D) SCO CPs have been designed. Furthermore, the 3D polymeric structure can add a nanoporous function.[3]

As stated above, the Hofmann-like CP series that formulated $M^1(L)_x[M^2(CN)_4]$ and $M^1(L)_x[M^3(CN)_2]_2$ (M^1 = Mn(II), Fe(II), Co(II), Ni(II), Cd(II), Zn(II), M^2 = Ni(II), Pd(II), Pt(II),[4] M^3 = Ag(I) or Au(I),[5] L = pyridine derivatives, x = 1 or 2) is the most convenient motif, which strongly defined the dimensionality depending on using monodentate or bidentate pyridine ligands. This motif consists of an octahedral metal ion (M^1) through N atoms of the cyanometalate unit at the equatorial position, building up an almost square mesh layer structure woven by $-M^1-N-C-M^{2,3}-C-N-M^1-$ infinite chains and monodentate pyridine (py) ligands at axial positions where it is vertical to the layer. A gap inside the square is penetrated by py ligands from the upper and lower layers, resulting in a parallel stacking array. The 3D structure can be also formed by using a pillared bidentate ligand. One of the best discoveries of the 3D Hofmann-like structure is Fe(pyrazine)$[M^2(CN)_4]$. This has a novel SCO property and trim nanoporous space, in which several interesting functionalities and applications were reported.[6] Such an excellent structural consistency gives us controlling dimensionality and functionality. Particularly, since 2000, many 2D bilayer structures $Fe^{II}(L)_2[M^3(CN)_2]_2$ have been developed. This series has an outstandingly similar crystal structure. However, the applicable monodentate ligands for the Hofmann-like 2D layer system are still determinative, which are only three- and/or four-substituent pyridine derivatives. So far, the 3-X-5-Ypyridine ligand produces a different unexpected structure. For example, SCO CP Fe(3,5-CH_3py)$_2[Ag_2(CN)_3][Ag(CN)_2]$ has been reported.[7] It is noted that the unique $[Ag_2(CN)_3]^-$ dimeric building block is generated by the dissociation equilibrium from the solution of $K[Ag(CN)_2]$ as follows:

$$[Ag(CN)_2]^- \leftrightarrow CN^- + AgCN \quad (1)$$

Received: February 18, 2021
Accepted: April 20, 2021
Published: April 29, 2021

Table 1. Crystallographic Parameters for 1−3[a]

	1 (296 K)	1 (90 K)	2 (275 K)	2 (90 K)	3 (275 K)	3 (90 K)
empirical formula	$C_{17}H_{12}Ag_3FeBr_2N_7$	$C_{17}H_{12}Ag_3FeBr_2N_7$	$C_{15}H_6Ag_3FeBr_2Cl_2N_7$	$C_{15}H_6Ag_3FeBr_2Cl_2N_7$	$C_{17}H_{12}Ag_3FeBr_4N_7$	$C_{15}H_6Ag_3FeBr_4N_7$
FW	853.62	853.62	894.418	894.418	983.37	983.37
crystal system	monoclinic	monoclinic	monoclinic	monoclinic	monoclinic	monoclinic
space group	*C*2/*c*	*C*2/*c*	*C*2/*c*	*C*2/*c*	*C*2/*c*	*C*2/*c*
a (Å)	12.7439(7)	12.4157(6)	12.7896(11)	12.4285(11)	12.806(11)	12.4670(14)
b (Å)	13.6462(8)	13.2373(7)	13.5068(11)	14.328(4)	13.584(11)	13.3156(15)
c (Å)	14.0322(8)	13.6566(7)	13.9946(12)	14.652(4)	13.973(11)	13.6789(15)
β (°)	101.1156(10)	100.2930(10)	100.9217(15)	100.2040(10)	100.781(14)	100.331(2)
V (Å^3)	2394.5(2)	2208.35(19)	2373.7(3)	2190.9(3)	2388(3)	2234.0(4)
Z	4	4	4	4	4	4
final *R* indices [*I* > 2sigma(*I*)]	R_1 = 0.0447	R_1 = 0.0303	R_1 = 0.0337	R_1 = 0.0272	R_1 = 0.0272	R_1 = 0.0261
	wR_2 = 0.1965	wR_2 = 0.0647	wR_2 = 0.1219	wR_2 = 0.0520	wR_2 = 0.0679	wR_2 = 0.611
R indices (all data)	R_1 = 0.0557	R_1 = 0.0323	R_1 = 0.0444	R_1 = 0.0381	R_1 = 0.0357	R_1 = 0.0325
	wR_2 = 0.1913	wR_2 = 0.0652	wR_2 = 0.1112	wR_2 = 0.0496	wR_2 = 0.0651	wR_2 = 0.0591

[a] $R = (\Sigma||Fo| - |Fc||)/\Sigma|Fo|$ $wR = \{\Sigma w(|Fo| - |Fc|)^2/\Sigma w|Fo|^2\}^{1/2}$.

$$AgCN + [Ag(CN)_2]^- \leftrightarrow [Ag_2(CN)_3]^- \quad (2)$$

As a result, existing two types of cyanometalate moieties are simultaneously assembled, demonstrating a new type of framework. In recent years, some examples by using the $[Ag_2(CN)_3]^-$ unit were reported.[8] Although an isostructural series of $Fe^{II}(L)_2[Au(CN)_2]_2$ and $Fe^{II}(L)_2[Ag(CN)_2]_2$ have been much reported, the $[Au_2(CN)_3]^-$ unit is still not found. Thus, the $[Ag_2(CN)_3]$ species is a rare building unit. The chain longer than $[Ag(CN)_2]$ can be utilized for a new variety of cyano-bridged motifs. These new prototypical structures show the variety of the SCO behavior. However, how to systematically design and control its structure such as the traditional Hofmann-like structure is still not found. In this paper, we report the synthesis, crystal structures, and physical properties of three novel CPs incorporating the $[Ag^I_2(CN)_3]$ building unit based on the 3-Br-5-Xpyridine derivatives (X = Cl, Br, and CH_3; see Scheme S1), formulating Fe^{II}(3-Br-5-CH_3py)$_2[Ag^I_2(CN)_3][Ag^I(CN)_2]$ (**1**), Fe^{II}(3-Br-5-Clpy)$_2[Ag^I_2(CN)_3][Ag^I(CN)_2]$ (**2**), and Fe^{II}(3,5-Brpy)$_2[Ag^I_2(CN)_3][Ag^I(CN)_2]$ (**3**).

2. RESULTS

2.1. Overview of the Structure for 1−3. These 3D frameworks of Fe(3-Br-5-Xpy)$_2[Ag_2(CN)_3][Ag(CN)_2]$ are almost isostructural (Figure 1 and Figures S1 and S2). **1**−**3** in the HS and LS state crystallize in the monoclinic centrosymmetric space group *C*2/*c*. For **1**−**3**, the asymmetric unit consists of the FeN_6 coordination environment. Two 3-Br-5-Xpy ligands coordinate to the axial positions. The 3-Br and 5-X substituents are disordered to each other at the 3,5-position. Thus, the two 3-Br-5-Xpy ligands are crystallographically equivalent. The equatorial positions are occupied by two types of cyanometalate units, $[Ag(CN)_2]^-$ and $[Ag_2(CN)_3]^-$ (Figure 2 (HS state) and Figure S3 (LS state)). In $[Ag_2(CN)_3]^-$ units, the crystallographic discrimination of the central CN linking group between Ag ions in the N−C−Ag−(CN)−Ag−C−N unit is impossible due to the inversion center between them. Thus, the central cyano substituent coexists in Ag(2)−CN−Ag(2) and Ag(2)−NC−Ag(2) conformations, which must be a static disorder. Both $[Ag(CN)_2]^-$ and $[Ag_2(CN)_3]^-$ have linear coordination geometries, forming shorter chains −Fe−N−C−Ag−C−N−Fe− and longer chains −Fe−N−C−Ag−(CN)−Ag−C−N−Fe−, respectively. The shorter and longer chains formed the rectangular motifs $\{Fe[Ag_2(CN)_3]\}_2\{Fe_2[Ag(CN)_2]_2\}_2$. The Fe···Fe distance in the shorter side of the rectangular moiety is ca. 15 Å, while the longer side is ca. 20 Å. The rectangles are perpendicularly connected to form a 3D network just like a piled brick wall (Figure 3). The intraframework spaces are occupied by two other identical but independent frameworks, which interpenetrate to each other (Figure S4). The Fe−N bond lengths for **1**−**3** correspond to the usual values for the Fe^{II} 100% HS state and 100% LS state (average Fe−N bond lengths for **1** = 2.164(4) Å (296 K), 1.956(3) Å (90 K), for **2** = 2.158(4) Å (275 K), 1.957(3) Å (90 K), and for **3** = 2.155(3) Å (275 K), 1.969(3) Å (90 K)). Close Ag···Ag distances between each frameworks indicate strong argentophilic interactions (see Figure 1), which is less than the sum of the van der Waals radius of Ag (ca. 3.60 Å). The py rings are stacked parallel to one another, which exhibits *π*-stacking interactions with displaced a stacking arrangement (Figure 4). The shortest contact $C_{py}\cdots C_{py}$ distances are 3.361(8) [3.271(6)] Å at 296 K [90 K] for **1**, 3.359(10) [3.280(4)] Å at 275 K [90 K] for **2**, and 3.345(7) [3.273(4)] Å at 275 K [90 K] for **3**. Furthermore, significantly smaller distances between Ag and X(Br) are also observed (Figure 4). These additional interactions increase dimensionality. The distances are gathered in Table 2.

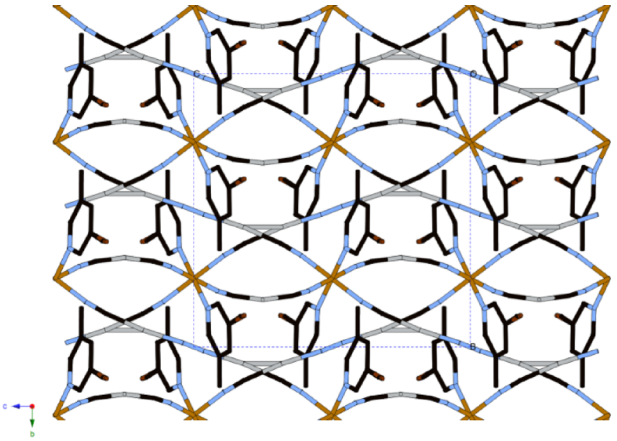

Figure 1. Crystal structure of **1** at 300 K. Short Ag···Ag contacts, as indicated by gray sticks. In this picture, hydrogen atoms are omitted for clarity.

https://doi.org/10.1021/acsomega.1c00892
ACS Omega 2021, 6, 12187−12193

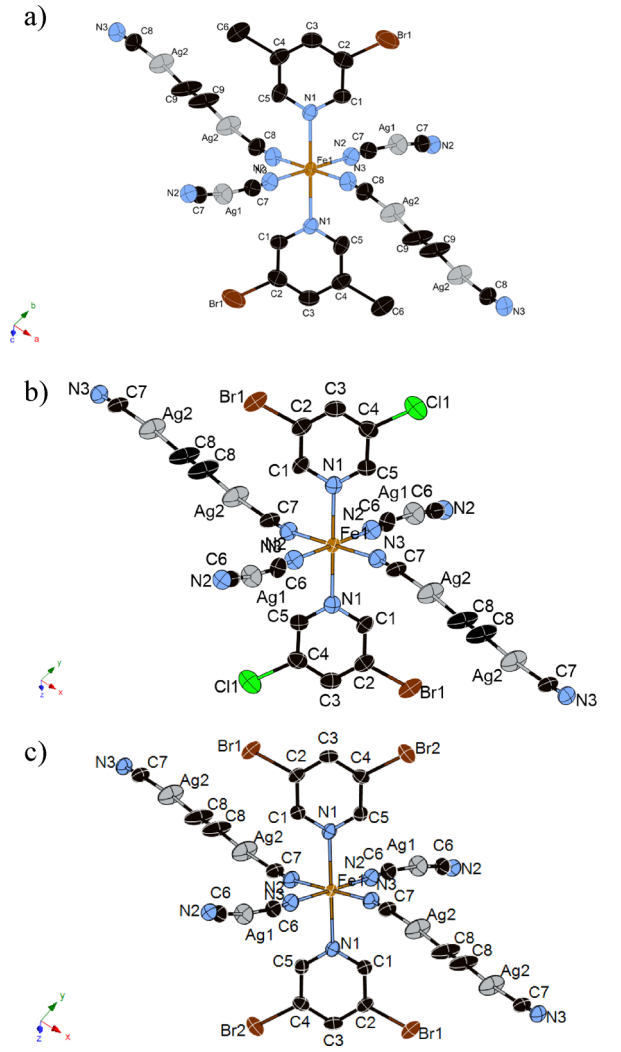

Figure 2. Molecular fragment of **1** at 275 K (a), **2** at 275 K (b), and **3** at 275 K (c). In these pictures, hydrogen atoms are omitted for clarity. The image showing Ag(2)−C−C−Ag(2) in the $[Ag_2(CN)_3]$ unit means the disorder model in −C−N− and −N−C− conformations.

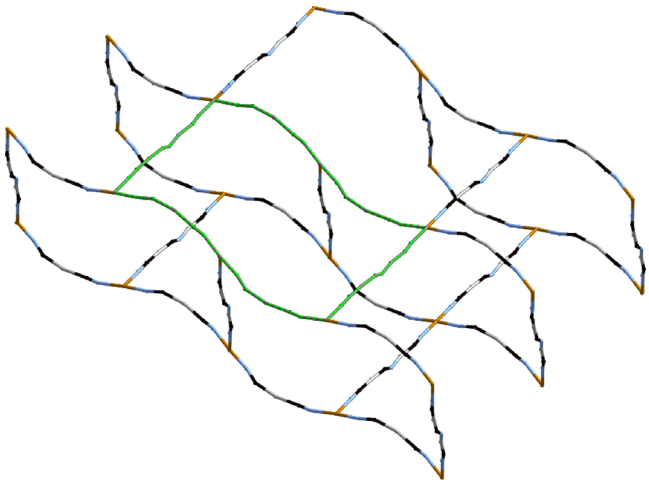

Figure 3. Schematic showing the 3D framework. Green lines indicate the one rectangular face of $\{Fe[Ag_2(CN)_3]\}_2\{Fe_2[Ag(CN)_2]_2\}_2$.

Interestingly, Ag···Ag contacts are also drastically changed by the spin transition. The changes of Ag···Ag distances upon

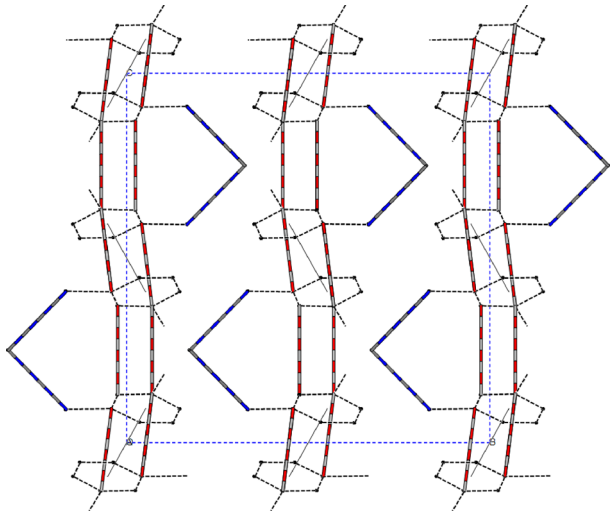

Figure 4. Representation of intermolecular short contacts of $C_{py}\cdots C_{py}$ (red cylinder lines) and Ag···X (blue cylinder lines) of **2**. Black lines show the shortest distances between the centroid of the rings. In this picture, hydrogen atoms are omitted for clarity.

Table 2. Selected Close Ag···Ag, $C_{py}\cdots C_{py}$, and Ag···X Distances [Å] of 1−3

	1 (293 K)	**1** (90 K)	**2** (275 K)
Ag···Ag	Ag(2)···Ag(2): 3.2546(16)	Ag(2)···Ag(2): 3.0995(13)	Ag(2)···Ag(2): 3.2751(22)
$C_{py}\cdots C_{py}$	C(2)···C(4): 3.480(10)	C(2)···C(4): 3.399(6)	C (2)···C(4): 3.459(11)
	C(3)···C(3): 3.361(8)	C(3)···C(3): 3.271(6)	C(3)···C(3): 3.359(10)
Ag···X	Ag(1)···Br(1): 3.5223(19)	Ag(1)···Br(1): 3.4582(16)	Ag(1)···Cl(1): 3.5142(24)
	2 (90 K)	**3** (275 K)	**3** (90 K)
Ag···Ag	Ag(2)···Ag(2): 3.1211(14)	Ag(2)···Ag(2): 3.2781(191)	Ag(2)···Ag(2): 3.1264(26)
$C_{py}\cdots C_{py}$	C(2)···C(4): 3.399(5)	C(2)···C(4): 3.444(14)	C(2)···C(4): 3.408(5)
	C(3)···C(3): 3.280(4)	C(3)···C(3): 3.345(7)	C(3)···C(3): 3.273(4)
Ag···X	Ag(1)···Br(1): 3.4626(14)	Ag(1)···Br(2): 3.5253(185)	Ag(1)···Br(2): 3.4971(26)

the spin transition are 0.1551(10) (**1**), 0.1540(13) (**2**), and 0.1517(96) (**3**) Å. On the other hand, Ag···X and $C_{py}\cdots C_{py}$ distances are slightly changed.

2.2. Magnetic Behaviors. Figure 5 shows the thermal dependence of $\chi_M T$ for **1**−**3**. The spin transition behaviors of **1**−**3** are almost similar. For **1**, at room temperature, $\chi_M T$ was 3.52 $cm^3 \cdot K \cdot mol^{-1}$. Upon cooling, $\chi_M T$ remains almost constant down to 280 K; below this temperature, $\chi_M T$ decreases to 0.42 $cm^3 \cdot K \cdot mol^{-1}$ at 212 K (T_c = 240 K), exhibiting an almost complete one-step spin transition. The observed second decrease in the residual value of $\chi_M T$ at a lower temperature of around 20−2 K is due to the typical behavior of zero-field splitting (ZFS). $\chi_M T$ values for **2** and **3** were 2.85 and 3.53 $cm^3 \cdot K \cdot mol^{-1}$ at room temperature, respectively. Like in **1**, **2** and **3** also show a sharp one-step spin transition. The critical temperatures are T_c = 249 K (**2**) and 250 K (**3**).

2.3. DSC Measurement. Spin transition behaviors were also confirmed by differential scanning calorimetry (DSC) measurement, as shown in Figure 6. DSC curves for **1**−**3** show anomalous peaks ($T_c^{\downarrow}$ = 235.0 K (**1**), 246.7 K (**2**), and 247.5 K

https://doi.org/10.1021/acsomega.1c00892
ACS Omega 2021, 6, 12187−12193

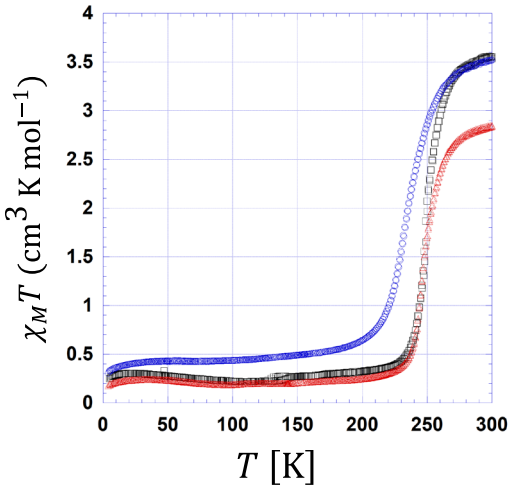

Figure 5. Temperature dependence of the magnetic susceptibilities for **1** (blue), **2** (red), and **3** (black).

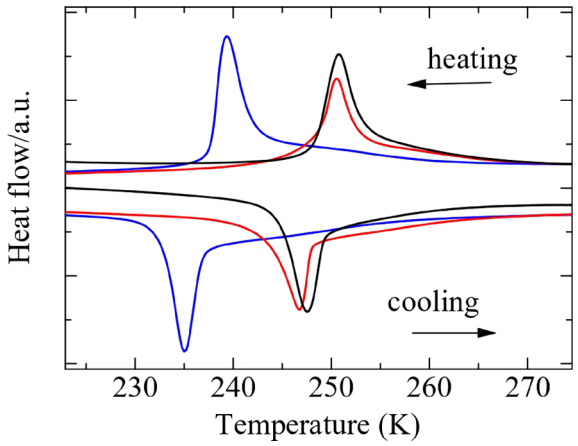

Figure 6. DSC curves of **1** (blue line), **2** (red line), and **3** (black line).

(**3**) and $T_c^{\uparrow}$ = 239.3 K (**1**), 250.5 K (**2**), and 250.8 K (**3**)). The average enthalpy and entropy variations associated with the cooling and heating modes obtained from these DSC curves, ΔH = 19.5 kJ·mol^{-1} (**1**), 18.0 kJ·mol^{-1} (**2**), and 21.1 kJ·mol^{-1} (**3**) and ΔS = 82.5 J·K^{-1}·mol^{-1} (**1**), 72.1 J·K^{-1}·mol^{-1} (**2**), and 85.1 J·K^{-1}·mol^{-1} (**3**), are in the range of typical values for cooperative SCO Fe^{II} compounds.

3. DISCUSSION

The previously reported compound of Fe(3,5-CH_3)$_2$[Ag$_2$(CN)$_3$][Ag(CN)$_2$] (**4**) is crystallographically identical (see Table S2) to **1**−**3**, also discussed in this paper. These compounds are only different in substituents. In terms of the dissociation equilibrium, although the precursor [Ag(CN)$_2$] is thermodynamically more stable than [Ag$_2$(CN)$_3$], the [Ag$_2$(CN)$_3$] species is the main product. The reason for the main product of Fe(L)$_2$[Ag(CN)$_2$][Ag$_2$(CN)$_3$] is due to the differences of stability of the crystal structure. In the case of Fe(L)$_2$[Ag(CN)$_2$]$_2$, the width of the 3,5-position substituents collides with the edge of the "square" window of {Fe$_2$[Ag(CN)$_2$]$_2$}$_4$. On the other hand, the wider "rectangular" window of {Fe[Ag$_2$(CN)$_3$]}$_2${Fe$_2$[Ag(CN)$_2$]$_2$}$_2$ easily penetrates the rectangle window. As a result, the crystal packing is stabilized. Therefore, the dissociation equilibrium (AgCN + [Ag(CN)$_2$]$^-$ ↔ [Ag$_2$(CN)$_3$]$^-$) is shifted to the right side.

Cell volumes, T_c, and related substituent parameters (the Hammett constant and Tolman cone angle) for **1**−**4** are listed in Table 3. The order of cell volumes is as follows: **2** (2373.7(3) Å^3) < **4** (2381.0(3) Å^3) < **3** (2388(3) Å^3) < **1** (2394.5(2) Å^3). In the view point of the substituent size, for example, considering the Tolman cone angles[9] (−CH_3 (90°) < −Cl (102°) < −Br (105°)), it seems that there are no relationships between the cell volume and substituent size. On the other hand, the series of the traditional 2D Hofmann layer structure of Fe(L)$_2$[M^3(CN)$_2$]$_2$ clearly shows a lattice expansion with the increase of the substituent size. The difference between the 2D layer type and the present 3D type is that there might be a margin of void space for **1**−**4** to accept the bulky substituents, while the interlayer space of the 2D layer type is relatively tight. In the view point of the electronic effect, the order of T_c has considerable relationships according to the Hammett constants[10] as follows: **4** (235 K) < **1** (240 K) < **2** (249 K) ≈ **3** (250 K) (Figure S5). The electron-donating substituent group (σ_p < 0) enhances the d−π interaction, decreasing Δ_o. Therefore, the −CH_3 substituent results in a relatively lower T_c. On the other hand, electron-withdrawing substituents (σ_p > 0) induce a higher T_c. The σ_p values of −Cl and −Br have the same positive values; therefore, the T_c values for **2** (3-Br-5-Cl-) and **3** (3-Br-5-Br-) are actually almost the same. Due to the complete isostructures of **1**−**4**, the order of T_c must be only considered and directly reflected to the substituent effect inducing electron-accepting/electron-donating properties.[11] In the previous papers, the synthesis and characterization of related compounds by using [Ag$_2$(CN)$_3$], {Fe(L)[Ag(CN)$_2$][Ag$_2$(CN)$_3$]}·nG (L = pyrimidine (L^1)[8a], 1,4-di(pyridin-4-yl)benzene (L^2)[8b], 2,6-naphthyridine (L^3)[8c], and 1,2,4,5-tetrakis(pyridin-4-ylethynyl)benzene (L^4)[8d]), have been reported. These compounds utilize bridging bi(L$^{1-3}$)- or tetra(L^4)-dentate ligands, forming quite different crystal structures to each other. On the other hand, **1**−**4** have monodentate ligands with a similar shape, forming an isostructure. T_c values for **1**−**4** are generally higher than previous compounds, L^1: T_{c1} = 185 K, $T_{c2}^{\uparrow}$ = 147.5, $T_{c2}^{\downarrow}$ = 146 K, L^2 (G = DMF·EtOH): $T_{c1}^{\uparrow}$ = 245 K, $T_{c1}^{\downarrow}$ = 218 K, L^2 (G = partially desorbed): $T_{c1}^{\uparrow}$ = 245 K, $T_{c1}^{\downarrow}$ = 218 K T_{c1} = 185 K, T_c = 150 K, L^2 (desorbed): T_c = 250 K, L^3: $T_c^{\uparrow}$ = 195 K, $T_c^{\downarrow}$ = 189 K, and L^4: T_c = 187 K. The ligands L$^{1-4}$ are relatively longer and bulky and have a complicated shape. Therefore, the higher T_c for **1**−**4** would be due to the denser crystal packing than those of L$^{1-4}$. Consequently, the dense packing induces a higher chemical pressure, increasing the ligand field strength Δ_o.

Table 3. Cell Volumes (HS State) and T_c of {Fe(3-Y-5-Xpy)$_2$[Ag^I(CN)$_2$]$_2$} and the Hammett Constant

substituents (Y, X)	ref	cell volume (Å^3)	average T_c (K)[a]
X, Y = −CH_3	6	2381.0(3)	235 K
X = −CH_3, Y = −Br	this work	2394.5(2)	240 K
X = −Cl, Y = −Br	this work	2373.7(3)	249 K
X = −Br, Y = −Br	this work	2388(3)	250 K
	−CH_3	−Cl	−Br
Hammet constant σ_p[9]	−0.17	0.23	0.23

[a]From the magnetic measurement.

https://doi.org/10.1021/acsomega.1c00892
ACS Omega 2021, 6, 12187−12193

4. CONCLUSIONS

New 3D network coordination polymers were reported. The present 3D structure was strongly defined by the substituent position, which would systematically design crystal structures and physical properties. Although this complicated 3D network includes various intermolecular interactions, there are no apparent hysteresis loops. It may be caused by longer chain −Fe−N−C−Ag−(CN)−Ag−C−N−Fe−, which separated the Fe···Fe distance and weakened cooperativities. However, the new series of spin crossover family as the Hofmann-like structure is still useful for investigating and modifying the spin crossover phenomena.

5. EXPERIMENTAL SECTION

5.1. Synthesis of 1−3. Freshly prepared single crystals of **1**−**3** were synthesized by slow diffusion of two solutions, one of which contained a mixture of $Fe(BF_4)_2{\cdot}6H_2O$ (33.7 mg, 1.00×10^{-4} mol) and each contained pyridine ligands (2.00×10^{-4} mol) in 1 mL of a water/ethanol mixed solvent. The others contained a water solution of $K[Ag(CN)_2]$ (20.0 mg, 1.00×10^{-4} mol) in 2 mL of water. The two solutions filled the glass tube. Yellow (**1** and **2**) and brown (**3**) single crystals suitable for single-crystal X-ray diffraction were formed over 2−4 days. The crystalline sample was picked up using a binocular lens. Due to the very small amount of crystals and mixed few impurities in the glass tube for **1** and **2**, the powder samples for a superconducting quantum interference device (SQUID), X-ray powder diffraction (XRPD), and elemental analysis were also prepared. For preparing the powder sample, one of these contained a mixture of $FeCl_2{\cdot}4H_2O$ (119.3 mg, 6.00×10^{-4} mol) and ascorbic acid (105.67 mg, 6.00×10^{-4} mol) in 5 mL of water. The others contained pyridine ligands (1.20×10^{-3} mol) in 1 mL of ethanol. The two solutions were communicated. Then, the solution of $K[Ag^I(CN)_2]$ (240.00 mg, 1.20×10^{-3} mol) in 5 mL of water was added to the previous solution. Yellow powder samples of **1** and **2** were formed immediately. The powder samples were washed with a large amount of ethanol (ca. 500 mL). The powder sample was checked by XRPD data (see Figures S6−S8). No impurity and isomers were observed. Elem. Anal. Calcd for $C_{17}H_{12}FeN_7Ag_3Br_2$ (**1**): C, 23.92; H, 1.42; N, 11.48. Found: C, 23.68; H, 1.60; N, 11.31. IR (cm^{-1}): 2173 (νC≡N). Calcd for $C_{15}H_6Fe\,N_7Ag_3Br_2Cl_2$ (**2**): C, 20.14; H, 0.68; N, 10.96. Found: C, 19.86; H, 0.86; N, 10.75. IR (cm^{-1}): 2171 (νC≡N). Anal. Calcd for $C_{15}H_6FeN_7Ag_3Br_4$ (**3**): C, 18.32; H, 0.62; N, 9.97. Found: C, 17.70; H, 0.85; N, 9.48. IR (cm^{-1}): 2171 (νC≡N).

5.2. Structural Analysis. Data collection was performed on a BRUKER APEX SMART CCD area detector diffractometer for **1**−**3** with monochromated MoKα radiation (λ = 0.71073 Å) (Bruker, Billerica, MA, USA). A selected single crystal was carefully mounted on a thin glass capillary and immediately placed under a liquid-cooled N_2 stream. The diffraction data were treated using SMART and SAINT, and absorption correction was performed using SADABS.[12] The structures were solved using direct methods with SHELXTL.[13] All non-hydrogen atoms were refined anisotropically, and the hydrogen atoms were generated geometrically. Pertinent crystallographic parameters, bond lengths, and angles for **1**−**3** are displayed in Table 1 and Table S1. Crystallographic data were deposited at the Cambridge Crystallographic Data Centre (CCDC): deposition numbers CCDC-2062871 for compound **1** (296 K), CCDC-2062872 for **1** (90 K), CCDC-2062873 for **2** (275 K), CCDC-2062874 for **2** (90 K), CCDC-2062875 for **3** (275 K), and CCDC-2062876 for **3** (90 K). These data can be obtained free of charge via http://www.ccdc.cam.ac.uk/conts/retrieving.html.

5.2.1. Cation. These cif files show the alerts A "short inter D···A Contact" (PLAT430), which was caused by the crystallographic discrimination of the central CN linking group between the CN−Ag−(**CN**)−Ag−CN unit. Each C(N) and N(C) are generated by the symmetry operation. Therefore, this "short inter D···A Contact" does not exist.

5.3. Physical Measurements. We measured the temperature dependence of the magnetic susceptibility of complexes **1**−**3** in the temperature range of 2−300 K with a cooling and heating rate of 2 K·min^{-1} in a 1 kOe field on a Quantum Design MPMS-XL SQUID magnetometer (Quantum Design, Inc., Pacific Center Court, San Diego, CA, USA). The diamagnetism of the samples and sample holders was considered. Calorimetric measurements were carried out using a differential scanning calorimeter Mettler Shimadzu DSC-60 in the temperature range of 215−285 K with a cooling and heating rate of 10 K·min^{-1}.

■ ASSOCIATED CONTENT

Supporting Information

The Supporting Information is available free of charge at https://pubs.acs.org/doi/10.1021/acsomega.1c00892.

Molecular structure of the used ligands (Scheme S1), powder diffraction data (Figures S6−S8), molecular fragments of **1**−**3** in the LS state (Figure S3), crystal structures of **2** and **3** (Figures S1 and S2), and thermal dependence of the HS fraction of **1**−**4** (Figure S5) (PDF)

Crystallographic data for **1**−**3** in the HS and LS state (ZIP)

■ AUTHOR INFORMATION

Corresponding Author

Takashi Kosone − *Department of Science and Engineering, Graduate School of Science and Engineering, Tokyo Denki University, Saitama 350-0394, Japan*; orcid.org/0000-0001-9403-8269; Phone: +81-49-296-2923; Email: t-kosone@mail.dendai.ac.jp

Authors

Syogo Okuda − *Department of Materials Science and Technology, Nagaoka University of Technology, Niigata 94-2188, Japan*

Masaya Kawata − *Department of Science and Engineering, Graduate School of Science and Engineering, Tokyo Denki University, Saitama 350-0394, Japan*

Shunsuke Arai − *Department of Science and Engineering, Graduate School of Science and Engineering, Tokyo Denki University, Saitama 350-0394, Japan*

Ryota Kosuge − *Department of Science and Engineering, Graduate School of Science and Engineering, Tokyo Denki University, Saitama 350-0394, Japan*

Takeshi Kawasaki − *Department of Chemistry, Faculty of Science, Toho University, Chiba 274-8510, Japan*

Complete contact information is available at: https://pubs.acs.org/10.1021/acsomega.1c00892

Author Contributions

T. Kosone, S.O., M.K., S.A., and R.K. carried out the synthesis. T. Kawasaki carried out the magnetic measurements and the structural analysis. T. Kosone interpreted and discussed the results.

Funding

This work was financially supported by KAKENHI (JSPS/18 K04964).

Notes

The authors declare no competing financial interest.

REFERENCES

(1) ((a)) Herrmann, W. A. *Transition Metal Coordination Chemistry*; Top. Curr. Chem, Springer, Berlin-Heidelberg-New York, 1992, Vol. *160* DOI: 10.1007/3-540-54324-4. ((b)) Albrecht-Schmitt, T. E. *Organometallic and Coordination Chemistry of the Actinides*, *Top. Curr. Chem*, Springer, Berlin-Heidelberg-New York, 2004, *Vol.* 127 DOI: 10.1007/978-3-540-77837-0. ((c)) Geoffrey, A. L. *Introduction to Coordination Chemistry*; *Inorganic Chemistry: A Textbook Series*, 2009, DOI: 10.1002/9780470687123 (d) Kitazawa, T. *Kagaku Kogyo* **2006**, *57*, 255−260.

(2) Gütlich, P.; Garcia, Y.; Goodwin, H. A. Spin Crossover Phenomena in Fe(II) Complexes. *Chem. Soc. Rev.* **2000**, *29*, 419−427.

(3) Kitagawa, S.; Kitaura, R.; Noro, S. Functional Porous Coordination Polymers. *Angew. Chem., Int. Ed.* **2004**, *43*, 2334−2375.

(4) (a) Kitazawa, T.; Gomi, Y.; Takahashi, M.; Takeda, M.; Enomoto, M.; Miyazaki, A.; Enoki, T. Spin-crossover behaviour of the coordination polymer $Fe^{II}(C_5H_5N)_2Ni^{II}(CN)_4$. *J. Mater. Chem.* **1996**, *6*, 119−121. (b) Niel, V.; Martinez-Agudo, J. M.; Muñoz, M. C.; Gaspar, A. B.; Real, J. A. Cooperative Spin Crossover Behavior in Cyanide-Bridged Fe(II)−M(II) Bimetallic 3D Hofmann-like Networks (M = Ni, Pd, and Pt). *Inorg. Chem.* **2001**, *40*, 3838−3839. (c) Agusti, G.; Cobo, S.; Gaspar, A. B.; Molnár, G.; Moussa, N. O.; Szilgyi, P.-.; Pálfi, V.; Vieu, C.; Muñoz, M. C.; Real, J. A.; Bousseksou, A. Thermal and light-induced spin crossover phenomena in new 3D Hofmann-like microporous metalorganic frameworks produced as bulk materials and nanopatterned thin films. *Chem. Mater.* **2008**, *20*, 6721−6732. (d) Martínez, V.; Gaspar, A. B.; Muñoz, M. C.; Bukin, G. V.; Levchenko, G.; Real, J. A. Synthesis and Characterisation of a New Series of Bistable Iron(II) Spin-Crossover 2D Metal−Organic Frameworks. *Chem. − Eur. J.* **2009**, *15*, 10960−10971. (e) Bartual-Murgui, C.; Ortega-Villar, N. A.; Shepherd, H. J.; Muñoz, M. C.; Salmon, L.; Molnár, G.; Bousseksou, A.; Real, J. A. Enhanced porosity in a new 3D Hofmann-like network exhibiting humidity sensitive cooperative spin transitions at room temperature. *J. Mater. Chem.* **2011**, *21*, 7217. (f) Ohtani, R.; Arai, M.; Hori, A.; Takata, M.; Kitao, S.; Seto, M.; Kitagawa, S.; Ohba, M. Modulation of Spin-Crossover Behavior in an Elongated and Flexible Hofmann-Type Porous Coordination Polymer. *J. Inorg. Organomet. Polym. Mater.* **2013**, *23*, 104−110. (g) Liu, W.; Wang, L.; Su, Y.-J.; Chen, Y.-C.; Tucek, J.; Zboril, R.; Ni, Z.-P.; Tong, M.-L. Hysteretic Spin Crossover in Two-Dimensional (2D) Hofmann-Type Coordination Polymers. *Inorg. Chem.* **2015**, *54*, 8711−8716. (h) Sciortino, N. F.; Zenere, K. A.; Corrigan, M. E.; Halder, G. J.; Chastanet, G.; Létard, J.-F.; Kepert, C. J.; Neville, S. M. Four-step iron(ii) spin state cascade driven by antagonistic solid state interactions. *Chem. Sci.* **2017**, *8*, 701−707.

(5) (a) Galet, A.; Muñoz, M. C.; Martinez, V.; Real, J. A. supramolecular isomerism in spin crossover networks with aurophilic interactions. *Chem. Commun.* **2004**, 2268−2269. (b) Muñoz, M. C.; Gaspar, A. B.; Galet, A.; Real, J. A. Spin-crossover behavior in cyanide-bridged iron(II)−silver(I) bimetallic 2D Hofmann-like metal−organic frameworks. *Inorg. Chem.* **2007**, *46*, 8182−8192. (c) Agust, G.; Muñoz, M. C.; Gaspar, A. B.; Real, J. A. Spin-crossover behavior in cyanide-bridged iron(II)−gold(I) bimetallic 2D Hofmann-like metal−organic frameworks. *Inorg. Chem.* **2008**, *47*, 2552−2561. (d) Kosone, T.; Kachi-Terajima, C.; Kanadani, C.; Saito, T.; Kitazawa, T. A two-step and hysteretic spin-crossover transition in new cyano-bridged hetero-metal $Fe^{II}Au^{I}$ 2Dimensional assemblage. *Chem. Lett.* **2008**, *37*, 422−423. (e) Kosone, T.; Kanadani, C.; Saito, T.; Kitazawa, T. Spin crossover behavior in two-dimensional bimetallic coordination polymer Fe^{II}(3-bromo-4-picoline)$_2[Au^{I}(CN)_2]_2$: Synthesis, crystal structures, and magnetic properties. *Polyhedron* **2009**, *28*, 1991−1995. (f) Kosone, T.; Tomori, I.; Kanadani, C.; Saito, T.; Mochida, T.; Kitazawa, T. Unprecedented three-step spin-crossover transition in new 2dimensional coordination polymer $\{Fe^{II}$(4-methylpyridine$)_2[Au^{I}(CN)_2]_2\}$. *Dalton Trans.* **2010**, *39*, 1719−1721. (g) Muñoz, M. C.; Real, J. A. Thermo-, piezo-, photo- and chemo-switchable spin crossover iron(II)-metallocyanate based coordination polymers. *Coord. Chem. Rev.* **2011**, *255*, 2068−2093. (h) Chiruta, D.; Linares, J.; Garcia, Y.; Dimian, M.; Dahoo, P. R. Analysis of multi-step transitions in spin crossover nanochains. *Phys. B* **2014**, *434*, 134−138. (i) Li, J.-Y.; He, C.-T.; Chen, Y.-C.; Zhang, Z.-M.; Liu, W.; Ni, Z.-P.; Tong, M.-L. Tunable Cooperativity in a Spin-Crossover Hoffman-like Metal−Organic Framework Material by Aromatic Guests. *J. Mater. Chem. C* **2015**, *3*, 7830−7835. (j) Kosone, T.; Kitazawa, T. Guest-dependent spin transition with long range intermediate state for 2-dimensional Hofmann-like coordination polymer. *Inorg. Chim. Acta* **2016**, *439*, 159−163. (K) Kosone, T.; Kawasaki, T.; Tomori, I.; Okabayashi, J.; Kitazawa, T. Modification of cooperativity and critical temperatures on a hofmann-like template structure by modular substituent. *Inorganics* **2017**, *5*, 55. (l) Delgado, T.; Meneses-Sánchez, M.; Piñeiro-López, L.; Bartual-Murgui, C.; Muñoz, M. C.; Real, J. A. Thermo- and Photo-Modulation of Exciplex Fluorescence in a 3D Spin Crossover Hofmann-Type Coordination Polymer. *Chem. Sci.* **2018**, *9*, 8446−8452. (m) Kosone, T.; Makido, Y.; Okuda, S.; Haigo, A.; Kawasaki, T.; Akahoshi, D.; Saito, T.; Kitazawa, T. Systematic Design of Crystal Structure for Hofmann-Like Spin Crossover Fe(L)2[Ag(CN)2]2 Complexes. *Crystals* **2019**, *9*, 370. (n) Piñeiro-López, L.; Valverde-Muñoz, F.-J.; Trzop, E.; Muñoz, M. C.; Seredyuk, M.; Castells-Gil, J.; da Silva, I.; Martí-Gastaldo, C.; Collet, E.; Real, J. A. Guest Induced Reversible on−off Switching of Elastic Frustration in a 3D Spin Crossover Coordination Polymer with Room Temperature Hysteretic Behaviour. *Chem. Sci.* **2021**, *12*, 1317−1326.

(6) (a) Ohba, M.; Yoneda, K.; Agustí, G.; Muñoz, M. C.; Gaspar, A. B.; Real, J. A.; Yamasaki, M.; Ando, H.; Nakao, Y.; Sakaki, S.; Kitagawa, S. Bidirectional Chemo-Switching of Spin State in a Microporous Framework. *Angew. Chem., Int. Ed.* **2009**, *48*, 4767−4771. (b) Kosone, T.; Hori, A.; Nishibori, E.; Kubota, Y.; Mishima, A.; Ohba, M.; Tanaka, H.; Kato, K.; Kim, J.; Real, J. A.; Kitagawa, S.; Takata, M. Coordination Nano-Space as Stage of Hydrogen Ortho−Para Conversion. *R. Soc. open sci.* **2015**, *2*, 150006.

(7) Kosone, T.; Suzuki, Y.; Ono, S.; Kanadani, C.; Saito, T.; Kitazawa, T. A New Spin Crossover Heterometallic $Fe^{II}Ag^{I}$ Coordination Polymer with the $[Ag_2(CN)_3]^-$ Unit: Crystallographic and Magnetic Study. *Dalton Trans.* **2010**, *39*, 1786.

(8) (a) Niel, V.; Thompson, A. L.; Goeta, A. E.; Enachescu, C.; Hauser, A.; Galet, A.; Muñoz, M. C.; Real, J. A. Thermal- and photoinduced spin-state switching in an unprecedented threedimensional bimetallic coordination polymer. *Chem. − Eur. J.* **2005**, *11*, 2047−2060. (b) Li, J.-Y.; Yan, Z.; Ni, Z.-P.; Zhang, Z.-M.; Chen, Y.-C.; Liu, W.; Tong, M.-L. Guest-effected spin-crossover in a novel threedimensional self-penetrating coordination polymer with permanent porosity. *Inorg. Chem.* **2014**, *53*, 4039−4046. (c) Piñeiro-López, L.; Valverde-Muñoz, F. J.; Seredyuk, M.; Bartual-Murgui, C.; Muñoz, M. C.; Real, J. A. Cyanido bridged Fe^{II}-M^{I} bimetallic Hofmann-like spincrossover coordination polymers based on 2,6-Naphthyridine. *Eur. J. Inorg. Chem.* **2018**, *2018*, 289−296. (d) Valverde-Muñoz, F. J.; Muñoz, M. C.; Ferrer, S.; Bartual-Murgui, C.; Real, J. A. Switchable Spin-Crossover Hofmann-Type 3D Coordination Polymers Based on Tri- and Tetratopic Ligands. *Inorg. Chem.* **2018**, *57*, 12195−12205.

(9) Tolman, C. A. Steric Effects of Phosphorus Ligands in Organometallic Chemistry and Homogeneous Catalysis. *Chem. Rev.* **1977**, *77*, 313−348.

(10) Hansch, C.; Leo, A.; Taft, R. W. A Survey of Hammett Substituent Constants and Resonance and Field Parameters. *Chem. Rev.* **1991**, *91*, 165−195.
(11) Kimura, A.; Ishida, T. Spin-Crossover Temperature Predictable from DFT Calculation for Iron(II) Complexes with 4-Substituted Pybox and Related Heteroaromatic Ligands. *ACS Omega* **2018**, *3*, 6737−6747.
(12) Sheldrick, G. M. *SADABS, Program for Empirical Absorption Correction for Area Detector Data*; University of Gttingen: Gttingen, Germany, 1996.
(13) Sheldrick, G. M. *SHELXL, Program for the Solution of Crystal Structures*, University of Gttingen, Gttingen, Germany, 1997.

https://doi.org/10.1021/acsomega.1c00892
ACS Omega 2021, 6, 12187−12193